J Mater Sci: Mater Med (2006) 17:1069–1078
DOI 10.1007/s10856-006-0533-8

Macroporous bioactive glass-ceramic scaffolds for tissue engineering

C. Vitale Brovarone · E. Verné · P. Appendino

Received: 13 July 2005 / Accepted: 24 October 2005

Abstract Highly bioactive scaffolds for tissue engineering were synthesized using a glass belonging to the SiO_2-CaO-K_2O (SCK) system. The glass SCK was prepared by a traditional melting-quenching route and its bioactivity was assessed by *in vitro* tests in a simulated body fluid (SBF). The glass was ground and sieved to obtain powders of specific size that were subsequently mixed with polyethylene particles of two different dimensions. The powders were then uniaxially pressed to obtain a crack free green compact that was thermally treated to remove the organic component and to sinter the inorganic phase. The obtained biomaterial was characterised by means of X-ray Diffraction, SEM equipped with EDS, mercury intrusion porosimetry, density measurements, image analysis, mechanical tests and *in vitro* evaluations. A glass-ceramic macroporous scaffold with a homogenously distributed and highly interconnected porosity was obtained. The amount and size of the introduced porosity could be tailored using various amounts of polyethylene powders of different size.

1 Introduction

The problem of bone loss and the need for bone grafts are ever increasing due to an increase in our life expectancy. In fact, bone grafts have many uses, e.g. bone loss or tumors, periodontal resorption, osteoporosis and arthroplasty revision surgery [1–3]. At present, autologous bone still represents the optimal material for a bone graft but its limited availability, the risk of donor site morbidity and the shape and size limitations should be borne in mind [4–6]. The use of allogenic/xenogenic implants also involves a nonzero potential of pathogen disease transmission and generally shows a bioresorption rate not compatible with the bone healing process [7–9]. Alternatives to autograft/allograft and xenograft are therefore highly desirable and are studied by many investigators. In fact artificial bone substitutes, being synthetic, overcome antigenicity and morbidity problems and can be available in unlimited amounts. Among alloplastic materials, a few ceramics ones are of particular interest due to their biocompatibility and osteoconductivity. These include hydroxyapatite and tricalcium phosphate, which have been widely investigated and are able to bond to bone *in vivo* but not to soft tissues [10–16]. Bioactive glasses and glass-ceramics of specific composition do represent a very attractive alternative. In fact they are biocompatible, bioactive, osteoconductive and even osteoproductive [10].

Their ability of creating a strong bond with the surrounding bone tissue is ascribed to a complex mechanism of ion exchange, silica gel formation and precipitation of a hydroxyapatite layer (HAp) on their surfaces when they are in contact with body fluids. This HAp layer has been shown to be very effective in promoting the osteointegration of the implant [17–19]. Besides it was recently discovered that the dissolution products of bioactive glasses exert a positive effect on the expression of genes regulating osteogenesis [20, 21]. An ideal scaffold should mimic the trabecular structure of bone and should act as a template on which cells can adhere, proliferate and promote the bone regeneration phenomena. A good osteointegration and vascularisation of the scaffold can be attained with an interconnected macro-porous network with pore diameters larger than 100 μm, though many authors agree that pores of a few hundred μm can be more effective [15, 22, 23]. Many methods [24] have been proposed to

C. V. Brovarone · E. Verné (✉) · P. Appendino
Politecnico di Torino, Materials Science and Chemical Engineering Department, Inorganic Composites and Advanced Ceramics, C.so Duca degli Abruzzi 24-I 10129 Torino, Italy
e-mail: enrica.verne@polito.it

prepare scaffolds for tissue engineering. Among them, starch consolidation [25–28], polymer foam replication [29, 30], direct foaming [31, 32], gel-casting [12] and solid freeform [23] have been widely investigated. Another method proposed in the literature involves the use of organic fillers that will be thermally removed. The organic fillers can be gelatine, camphor, sucrose or, as was in our case, polyethylene [33–35]. In this research work we choose the organic filler method to prepare macroporous bioactive scaffolds due to the high versatility of this method and its low-cost. A bioactive glass has been chosen to prepare the scaffolds due to its osteoproductive properties and to its potential in stimulating the ostoblasts proliferation with its dissolution products. Besides the high specific surface of the prepared scaffolds and the high reactivity of the chosen glass can be an effective way to produce a resorbable scaffold for tissue engineering.

2 Experimental procedure

2.1 Materials

In this research both organic and inorganic materials were used to obtain macroporous scaffolds through the burning out of the organic phase and the sintering of the inorganic one. The chosen inorganic phase is a bioactive glass belonging to the system SiO_2-CaO-K_2O with the following molar composition: 50%SiO_2-44%CaO-6%K_2O. The proposed glass was previously prepared and used with success by the authors to obtain bioactive coatings on alumina and Ti6Al4V [36] and will be from now on named SCK.

SCK was prepared by melting the raw products (SiO_2, $CaCO_3$, K_2CO_3) in a platinum crucible at 1500°C for 1 h and by quenching the melt in cold water to obtain a frit that was subsequently ground by ball milling and sieved to a final grain size below 106 μm (sieve of 140 mesh per inch).

This glass was thermally characterized in a previous work [36] where the thermal analysis pattern is reported. In that work the glass transition temperature($T_g = 720$°C), the crystallization of two phases at 800 and 820°C (with a decomposition signal at about 880°C) and of a third phase at 910°C (stable up to the instrumental limit, i.e. 1300°C) were evidenced and the linear expansion coefficient ($\alpha = 9.5 \times 10^{-6}/$°C) was reported. The softening range for this glass was around 900°C.

2.2 Scaffolds preparation

The scaffolds were prepared by mixing SCK powders with a thermally removable second phase. At this purpose, two different polyethylene particles, supplied by Wrigley Fibres (Somerset, United Kingdom) were used.

Briefly, SCK powders, sieved below 106 μm, were mixed with a proper amount of one of the two following polyethylene powders:

- PE1: particles size within 100–300 μm
- PE2: particles size within 300–600 μm

The powders were carefully mixed for 30′ in a plastic bottle using a rolls shaker in order to obtain an effective mixing.

Various amounts of PE1 or PE2 were added to SCK powders to produce different series of scaffolds. Specifically, the investigated polyethylene range was varied from 40 to 70%vol. for evaluating the optimal conditions for obtaining scaffolds with satisfactory mechanical strength and high porosity content. Polyethylene contents higher than 70% did not yield reproducible green compacts, and contents below 40% were considered too low to produce enough porosity. The prepared scaffolds will be named, from now on, with an acronym indicating the type and amount of used polyethylene particles: for instance PE1-40 (scaffolds obtained using 40%vol. of PE1 particles) or PE-50 to indicate generically the series of scaffolds realised using 50%vol. of polyethylene powders (they could be PE1-50 or PE2-50).

The green samples were obtained optimising the applied pressure and time aiming to obtain a crack free material: the best conditions were identified with a pressure of 150 MPa for 10 s using propanol as liquid binder. The green compacts were shaped in form of disks (3 cm diameter, 0.5 cm thickness) for the morphological and *in vitro* characterisation and in form of bars (5 cm × 1 cm × 1 cm) for the mechanical tests.

The green bodies were thermally treated aiming to remove the polyethylene powders while sintering the SCK ones to obtain a macroporous scaffold. The time and temperature of the thermal treatment (2 h at 950°C after introducing the green pieces in the furnace directly at the chosen temperature) were chosen on the basis of SCK characteristics and were optimised to allow a good sintering while avoiding an excessive softening of the glass that will cause the collapse of the structure and of the introduced porosity.

2.3 SCK characterisation

Aiming to characterise the *in vitro* bioactivity of the starting glass, SCK was also poured on a preheated stainless steel plate to produce bars. The bars were annealed for 12 h at 650°C and then cut in slices using a diamond blade in order to produce slices of 1 cm × 1 cm × 0.2 cm. The annealing temperature was chosen on the basis of previous thermal characterizations [36], and it was close to the glass-transition temperature of SCK. On the prepared slices the bioactivity was evaluated by soaking them in a simulated body fluid (SBF), which has almost the same ion concentrations as human plasma [37], for different times, from 1 week to 3 months. Specifically, the slices were soaked in 25 ml

of SBF in polyethylene bottles with a refresh of the solution every 48 h. To evaluate the formation of a silica rich layer and of hydroxyapatite (HAp) aggregates on the glass surface the slices were characterised, after different soaking periods, by X-ray diffraction (X'Pert Philips diffractometer) using the Bragg Brentano camera geometry and the CuK incident radiation. On the soaked slices, scanning electron microscopy (SEM Philips 525 M) with compositional analyses (EDS, Philips-EDAX 9100) were carried out to evaluate the amount and morphology of the precipitated HAp and its precipitation kinetics. The same investigations were carried out on SCK slices that underwent a treatment analogous to the optimised sintering one to ascertain eventual differences between the as prepared amorphous SCK and glass-ceramic SCK (GC-SCK).

In fact, the proposed sintering treatment is above the SCK crystallization temperature and thus the nucleation and growth of crystalline phases in the amorphous SCK will occur. The nature and morphology of the nucleated crystalline phases was investigated through X-ray diffraction and SEM equipped with EDS.

For the morphological and compositional studies, GC-SCK slices were chemically etched for 30 s with a 5%mol HF/HNO_3 (1:1) solution to remove the amorphous phase.

2.4 Scaffolds characterisation

On the prepared scaffolds a complete morphological characterisation was carried out through SEM investigations. Specifically the outer surfaces of the scaffolds were observed before and after polishing to evaluate the pore morphology and distribution, their degree of interconnection and the quality of the pore struts.

The cross sections of the scaffolds were also studied to evaluate the homogeneity of the pores distribution along the section as well as the degree of interconnection. SEM observations and comparison were carried out on the different scaffolds to evaluate the influence of the type and amount of polyethylene particles on the final quality of the scaffold (presence of dense sintering necks, pore distribution and amount). On the most representative samples, mercury intrusion porosimetry studies (FISONS macropores unit 120) were performed to acquire a quantitative evaluation of the amount and size of the obtained porosity. This technique allows the detection of pores of less than 100 μm diameter.

The total porosity (%) was also evaluated on 1 cm × 1 cm × 1 cm cubic samples through weight measurements knowing the SCK true density, by the following calculation: [1− (scaffold density/true density)] × 100.

Finally, for pores larger than 100 μm, image analysis studies (QWin Leica) were carried out to attain a quantitative evaluation of the pores size distribution and amount.

On the most promising scaffolds compressive tests were carried out on 3 cubic samples 1 cm × 1 cm × 1 cm using an Instron machine. The compressive strength was calculated from the maximum load registered during the test divided by the loaded area.

Moreover to study the isotropy of the prepared scaffold, the compressive strength was evaluated in the three directions to assess any eventual anisotropy.

Preliminary *in vitro* tests (soaking in SBF) were carried out on the scaffolds to verify the influence of the pores and of the higher specific surface involved. Samples of 1 cm^3 have been soaked in 25 ml SBF, in polyethylene bottles, with the same modalities described for bulk SCK.

3 Results and discussion

Figure 1a reports the as prepared SCK surface after 1 week in SBF. A silica gel covers the whole surface (the cracks are the result of SEM vacuum) and globular shaped agglomerates can be seen on top of it. The white agglomerates show the typical morphology of HAp precipitated from solutions. The morphological findings were integrated with EDS analyses to assess the composition of the whole surface (1b) and of the area in the white rectangle (1c). As shown by the compositional results, SCK surface after 1 week of soaking is manly composed by silica gel (Fig. 1b) and the globular shaped agglomerates can be identified as calcium phosphates (Fig. 1c).

The SCK surface modifications induced by soaking in SBF were further investigated by X-ray diffraction (Fig. 2). The as prepared SCK pattern shows only a broad halo confirming that the starting material was completely amorphous. After 1 week of soaking in SBF, the diffraction pattern shows a broad signal at 31–32° degrees and the presence of an amorphous halo, a few degrees lower. After 1 week of soaking the amorphous halo was detected at lower diffraction degrees than for the as-prepared SCK due to the formation of the silica gel layer on the SCK surface [38]. The peaks at 31–32° degrees two theta were identified with HAp and are broad due to the microcrystalline nature of HAp nucleated from solutions [39, 40]. For longer soaking periods (3 months), the signals of HAp became more intense due to a more complete covering of the SCK surface by HAp aggregates as confirmed also by morphological evaluations and compositional analyses.

The preparation of the scaffold involved a thermal treatment to remove the organic phase and to sinter the inorganic one. The chosen thermal treatment was above the SCK crystallisation temperatures and thus the nucleation and growth of one or more crystalline phases within the amorphous matrix will occur. The nucleation and growth of crystalline phases in a glass greatly influences its bioactivity. In fact, the crystal phase may or may not be bioactive and of course the residual amorphous phase differs, sometimes remarkably, from the

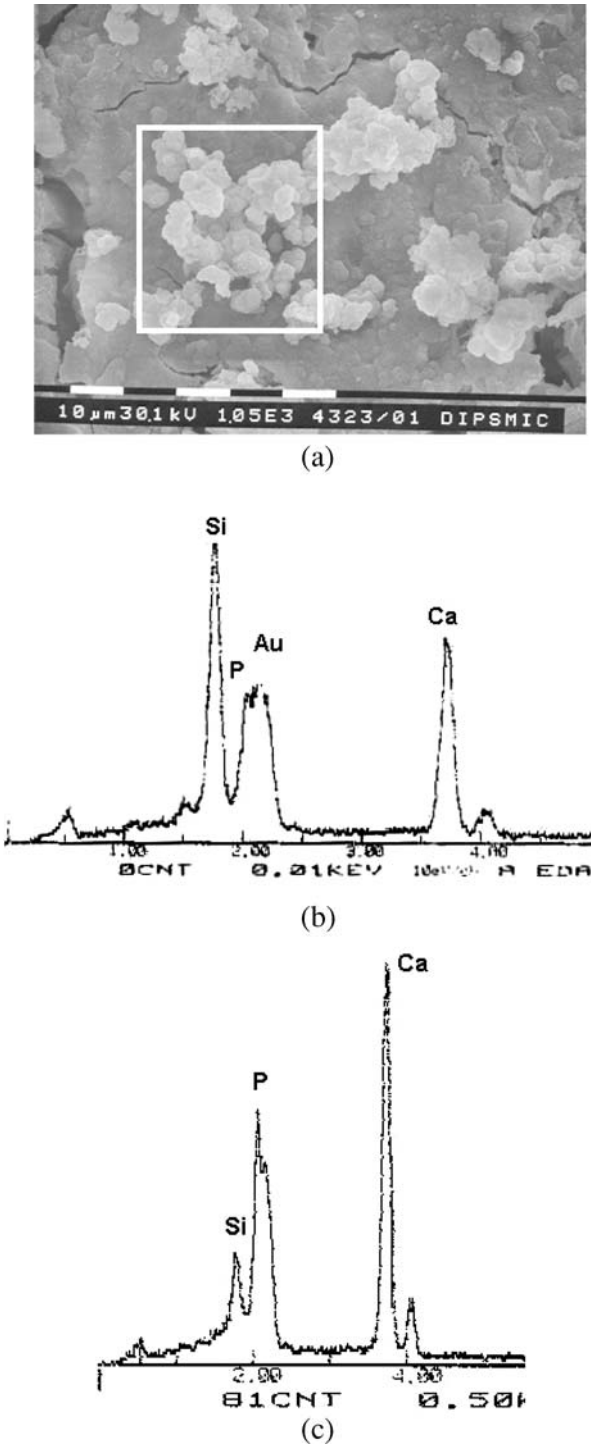

Fig. 1 Micrograph of SCK after 1 week in SBF (a), EDS analysis on the whole reported area (b), EDS analysis on the area in the rectangle (c).

original glass composition. For this reason, $1 \times 1\,cm^2$ SCK slices were cut and underwent a thermal treatment analogous to the optimised sintering one so that glass-ceramic samples were obtained (GC-SCK).

The presence of one or more crystalline phases, their morphology and composition were investigated through SEM equipped with EDS: only a crystalline phase containing Si and Ca was found. Figure 3a reports the morphology of the crystalline phase that, as can be observed, is present in great amounts.

The diffraction data, not reported here, were consistent with the compositional ones and identified the crystalline phase with β-wollastonite (β-$CaSiO_3$), which is known for its high bioactivity index [41, 42].

The GC-SCK *in vitro* bioactivity was investigated by soaking the samples in SBF for different periods, from 1 week up to 3 month. As can be observed in Figs. 3b and 3c GC-SCK is bioactive as on its surface after 1 week in SBF globular precipitates, identified as HAp, can be observed. In fact the EDS results showed the presence of Ca and P in proportion typical of HAp and of Si in lower amount due to the silica gel underneath it. The high bioactivity found both for as prepared SCK and for GC-SCK could be expected due to the presence of K^+ ions in the glass. The K^+ release occurs *in vitro* during the H^+/K^+ exchange phenomena that represent the first step of the bioctivity mechanism. K^+ have a quite large ionic radius (1.33 Å) if compared with the alkaline ions present in a traditional bioactive glass composition (es. Na^+, 0.95 Å) and thus their release into physiological fluid has a "disrupting" effect on the glass network highering its specific surface area and thus its reactivity.

On this basis and considering their high surface area, a bioactive behaviour of the scaffolds could be expected.

In this research the scaffolds were obtained using two organic phases thermally removable as pores former. The two organic phases consisted of PE powders that only differ for their sizes as can be seen in Figs. 4a and 4b where the micrographs of PE1 and PE2 are reported respectively. On the Wrigley Fibres Data Sheet, PE2 powders are said to be two times larger than PE1 ones, in good accordance to our SEM observations.

The minimum pore size allowing a proper bone in-growth is still under discussion, though most authors agree in fixing a minimum size of 100 μm and considering larger pores (for instance 300–500 μm) more effective. The pores amount and size greatly influences the final mechanical performances of a scaffold and thus using various type and amounts of PE can be an effective way for offering the best solution for different requirements and applications.

The optimized thermal treatment led to glass-ceramic macroporous scaffolds containing β-$CaSiO_3$, as verified by XRD.

PE1-40, PE2-40, PE1-50 and PE2-50 were the first prepared scaffolds and their morphology and mechanical strengths demonstrated that the PE-50 series maintain satisfactory properties.

Figure 5a shows the polished surface of PE1-50 where pores as large as 100–150 μm can be seen. As can be observed, the pores struts are thick and dense. Figure 5b shows

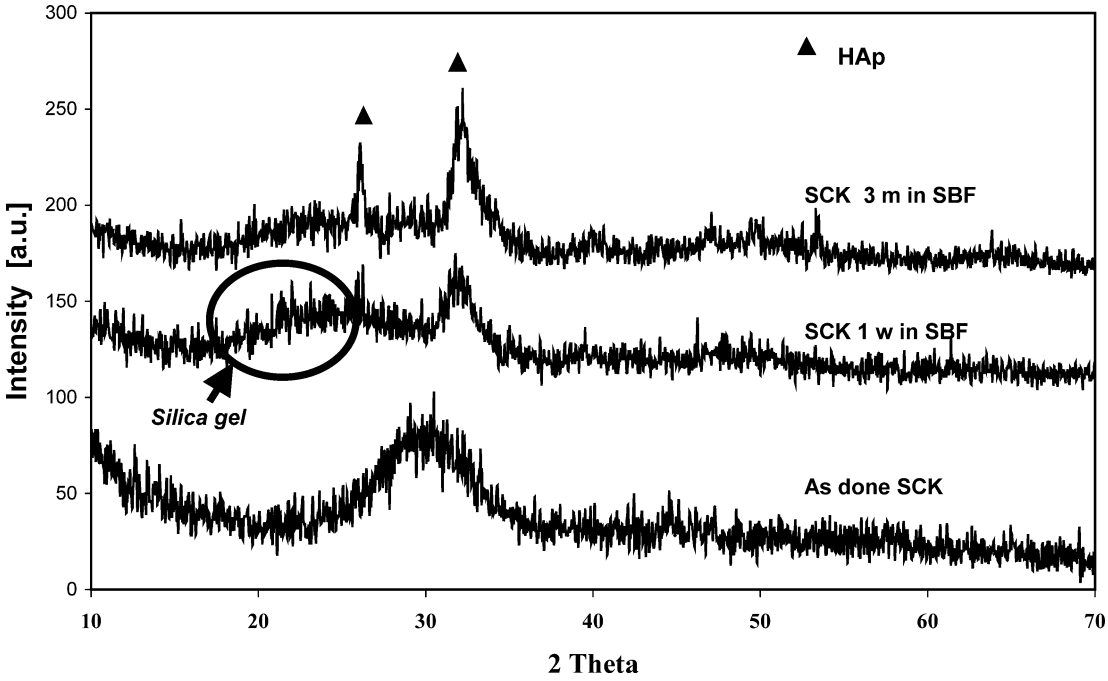

Fig. 2 Diffraction pattern of glassy SCK as done and after soaking in SBF for different periods of time (1 week and 3 months).

the as prepared surface of PE2-50, where pores as large as a few hundred microns can be observed. In this case, as the sample was not polished, the surface roughness of the scaffolds due to their glass-ceramic nature can be seen. The scaffolds roughness is crucial, as many investigators have assessed that osteoblasts prefer a rough surface [43]. Besides, smaller pores of only a few microns can be seen all over the surface and they are probably due to the CO_2 and H_2O gases coming out of the sample during the thermal treatment. The presence of micropores is an important feature of these scaffolds, as it is known that small pores favour cell adhesion and allow the physiological fluids to enter the inner part of the scaffold. The micrograph reported in Fig. 5b shows also the presence of other pores behind those on the foreground assessing the good interconnection degree of the prepared scaffolds. A high degree of interconnection is crucial to attain a fast and complete viability of the inner part of the scaffolds and thus to assure a complete and effective bone in-growth *in vivo*.

All the pores show dense sintering necks that can be observed rather well in the right bottom part of the micrograph (see arrows).

After this first analysis the organic content was higher till 60 and 70%vol, generating the PE-60 and PE-70 series. Figure 6a reports the cross section of PE2-60. The morphology of the cross section was particularly important to verify if the proposed method was suitable for obtaining homogenous scaffolds with pores distributed uniformly all over the sample. As can be seen in Fig. 6a, which is representative of what has been observed also for the other scaffolds, a homogenous pores distribution was attained. The homogenous distribution on the scaffold surface (Fig. 5) and on the cross sections, combined with the observed interconnection of the pores, was assessed for all the scaffolds.

All these features are of crucial importance when a good vascularisation of the scaffolds and a satisfactory biological viability of them are desired *in vivo*.

Generally, increasing the PE content will higher the pores amount but will also gradually lower the mechanical properties so that it is important to identify the maximum PE content allowing satisfactory mechanical strength of the scaffolds.

Figure 6b reports the PE2-70 surface morphology. In this case, the scaffolds struts are not well densified as the single SCK powders can be seen and thus poor mechanical strength will result. On this basis, 60%vol. was considered as the higher content of PE that allowed maintaining sufficient mechanical strength and obtaining dense pores struts.

The degree of pore interconnection as well as the presence of thick pores struts was further investigated through SEM observations at higher magnifications as can be seen in Figs. 7a and 7b respectively. The presence of a high amount of microporosity along with larger pores was assessed for every scaffold. Despite the presence of microporosity, which as explained before can play an important role *in vivo*, the pores struts are well sintered as the original SCK particles can not be distinguished.

The morphological observations were useful to assess the microstructure of the scaffolds, the pore morphology, interconnection and size. A quantitative pore-size distribution was performed, on the most representative samples, by mercury

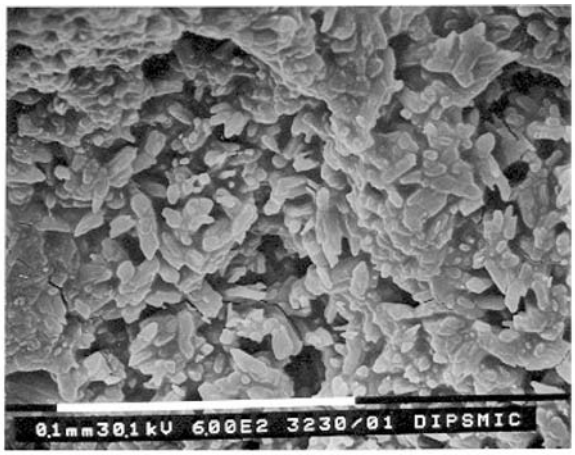

(a)

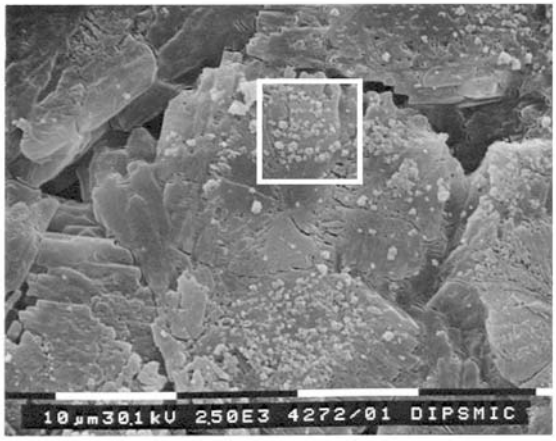

(b)

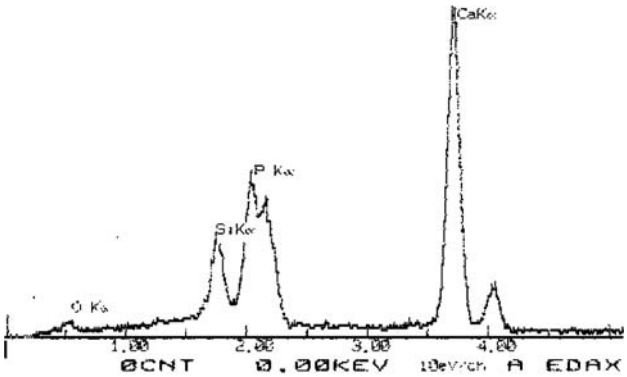

(c)

Fig. 3 Micrograph of GC-SCK after chemical etching (a), micrograph of GC-SCK after 1 week in SBF (b), EDS analysis on the area in the rectangle (c).

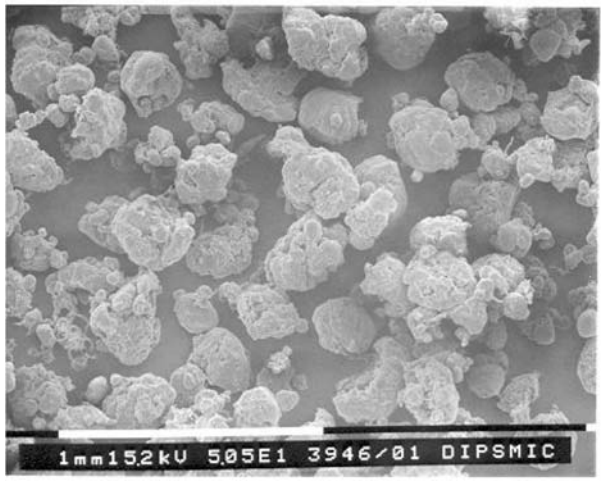

(a)

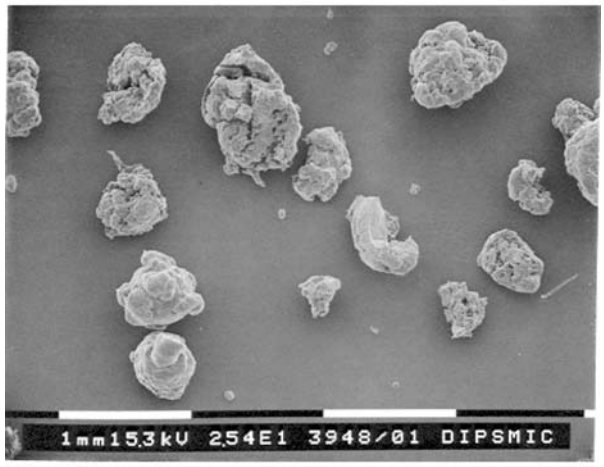

(b)

Fig. 4 Micrographs of the two different polyethylene powders: PE1 (a) and PE2 (b).

Table 1 Total porosity obtained via density measurements

Sample	Total porosity (vol.%)
PE1-50	60 ± 1
PE2-50	62 ± 1

intrusion porosimetry. This technique is useful to study the amount and pore size distribution of pores as large as 100 μm, but can not detect larger ones, as Hg, despite its very low wettability, enters inside them without any applied pressure. For this reason, the mercury intrusion porosimetry was used only to investigate the presence and size of the microporosity observed at SEM. Figure 8 reports the mercury intrusion porosimetry results obtained for PE1-50 that shows the presence of many micropores within 1–10 μm. The results obtained for the other scaffolds are analogous to the one reported for PE1-50. The presence of a high amount of small pores was ascribed to the removal of the polyethylene decomposition products, as the pores are open and accessible to Hg.

The total porosity was evaluated through weight measurements of cubic samples considering the SCK density. The calculated total porosity values for the most representative samples are reported in Table 1. As can be observed, the total porosity is slightly higher than the used PE content due to

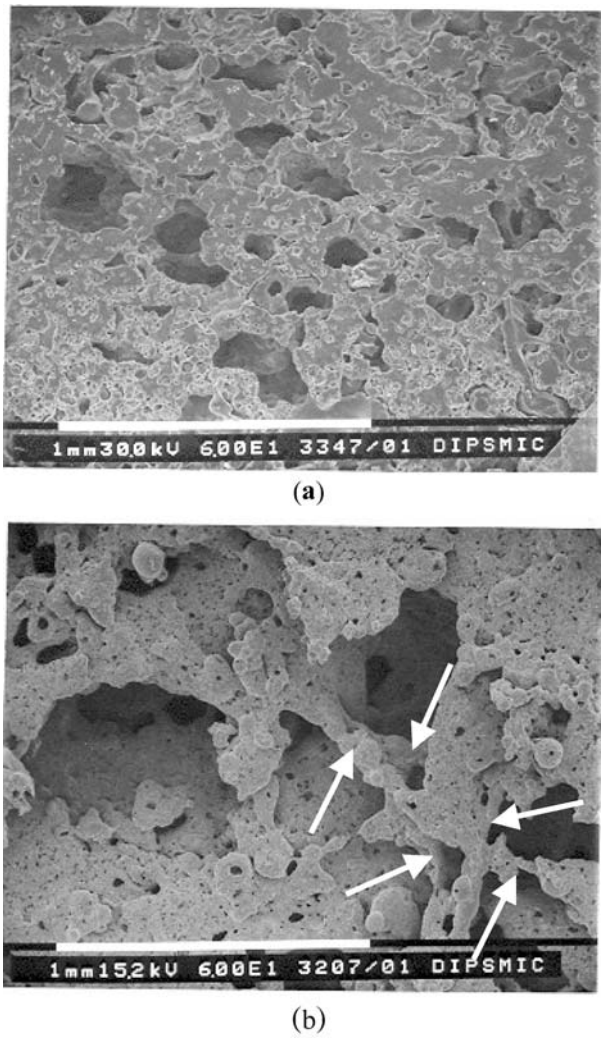

Fig. 5 Micrographs of the polished surface of PE1-50 (a) and of the as done PE2-50 surface (b).

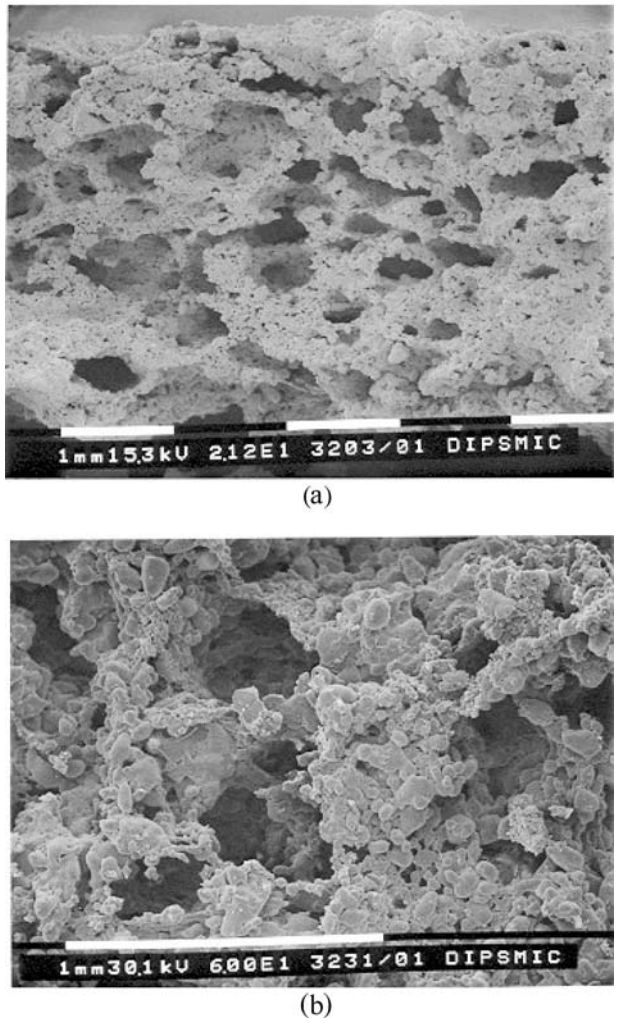

Fig. 6 Micrographs of a PE2-60 cross section (a) and of PE2-70 surface (b).

the removal of the decomposition products and the formation of micropores.

A more complete characterisation of the introduced porosity was attained through image analysis on polished sections of the scaffolds. In such a way the size and number of pores could be evaluated. At this purpose, Fig. 9a reports, as an example, a micrograph of PE2-50 in which the darker areas are pores that will be identified from the image analysis system as empty space. Figure 9b reports the results of the image analysis calculated considering, not the number of pores having a particular size, but the total area occupied by the pores having a specific size range, considering as 100% the whole pore area. The results were calculated in such a way considering that the total number of pores having a specific size range is not as important as the total empty volume and its mean size. In fact the crucial point is that the blood vessels and cells can easily penetrates inside the scaffold due to an elevated area of it occupied by sufficient large pores. Different areas were analysed obtaining comparable results.

Table 2 Compressive strengths of the scaffolds

Sample	Compressive strength (MPa)
PE1-50	6.0 ± 1.2
PE2-50	3.2 ± 1.1
PE1-60	1.8 ± 0.4
PE2-60	1.5 ± 0.5

The obtained results perfectly agree with the density data proving the reproducibility and the homogeneity of the prepared scaffolds. For the different samples, due to the PE content, a total porosity within 50 to 70%vol. was found.

The amounts, size of total porosity as well as the pore struts morphology are the main factors affecting the mechanical characteristics of the scaffolds. On the basis of the morphological observations, being the most promising samples, series PE-50 and PE-60 scaffolds were tested in compression using cubic samples of $1 \times 1 \times 1$ cm^3: the obtained results are reported in Table 2. As can be observed the standard

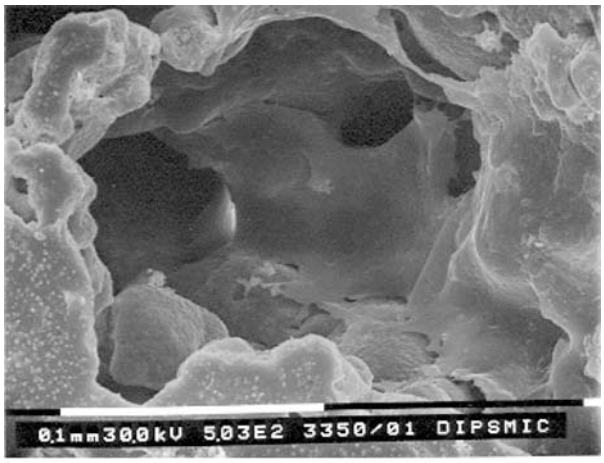

Fig. 7 Micrographs of PE1-50 (a) and PE2-50 (b).

deviation values are low indicating a good reproducibility of the samples. The series of PE1 scaffolds showed greater values compared to PE2 series with the same PE content due to the presence of larger pores in the latter ones.

An increase in the pores amount involved a decrease in the compressive strength: the decrease was less evident for PE2-60 scaffolds. On PE-50 and PE-60 series of scaffolds, the compressive strength was evaluated in the three directions to

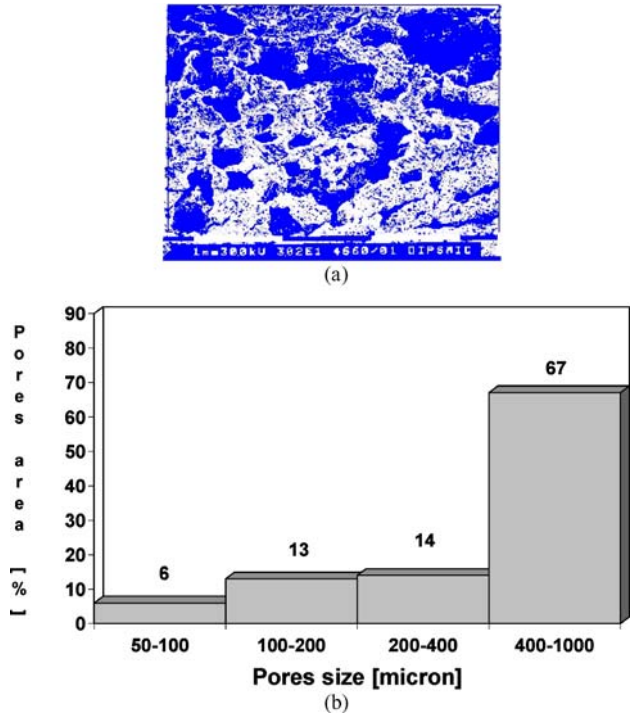

Fig. 9 Selected area for image analysis of sample PE2-50 (a), pores distribution for PE2-50 (b).

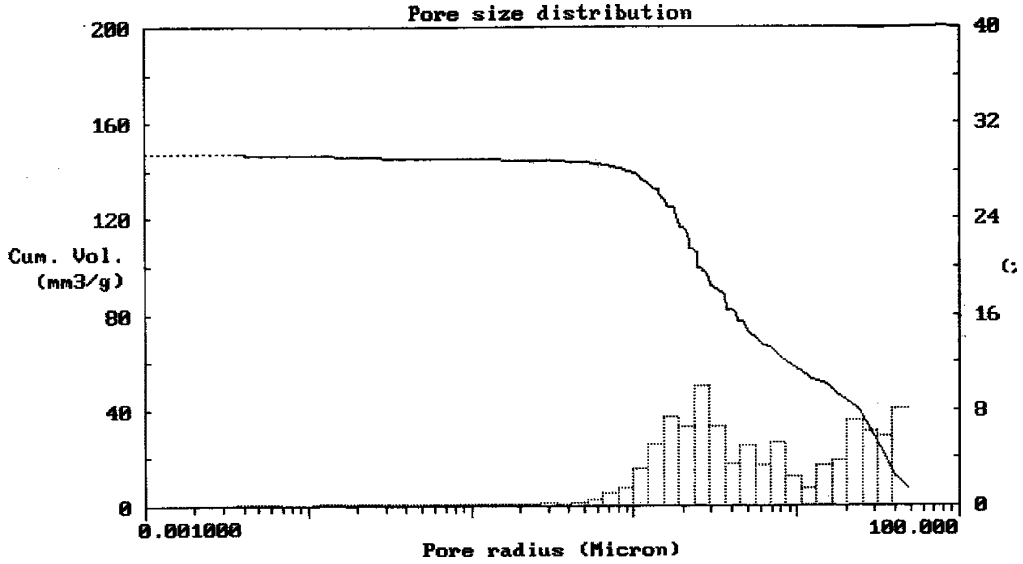

Fig. 8 Mercury intrusion porosimetric analysis of sample PE1-50.

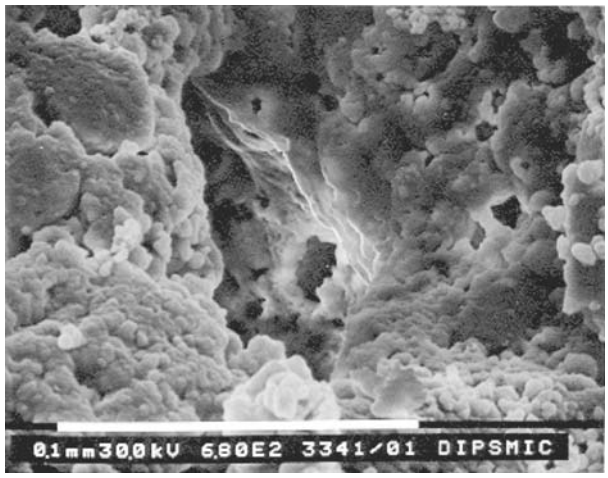

Fig. 10 Micrograph of PE2-50 after 1 week in SBF.

verify the homogeneity of the scaffolds and the isotropy of its properties. The obtained values were analogous in the three directions with differences not significant and well below the standard deviation. On the basis of the obtained results we could conclude that the observed scaffolds morphology and homogeneity corresponded to mechanical strength comparable to the ones reported in the literature for other scaffolds and for cancellous bones [3, 12, 23, 44, 45].

The *in vitro* bioactivity of the prepared scaffolds was assessed through soaking in SBF and many HAp agglomerates were observed after only one week in SBF. At this purpose, Fig. 10 reports a micrograph of PE2-50 after 1 week in SBF where HAp aggregates nucleated both outside and inside the pores can be seen. The scaffolds showed a stronger bioactivity than GC-SCK due to their higher specific surface reactivity.

4 Conclusions

Macroporous glass-ceramic scaffolds were produced via uniaxial pressing followed by a thermal treatment to remove the PE particle and to sinter the glass powders.

The pores were highly interconnected. The pores struts were thick and dense and the compressive strength of the scaffolds was about the strength of cancellous bone. An extensive microporosity was observed in all the scaffolds and can positively affect cell adhesion phenomena.

The introduced porosity was higher than 100 μm for series PE1 and above 200–500 μm for series PE2 scaffolds. The total pores amounts could be tailored within 50 to 70%vol.

The use of different polyethylene particles in various amounts showed to be an effective way to tailor the pores size and amount to the desired extent.

The scaffolds showed a great *in vitro* bioactivity due to the presence of β-wollastonite crystals, to the K^+ ions effect and to their high specific surface area.

The prepared scaffolds can be proposed as bone substitutes or can be used to vehicle osteoblasts, collagen or other biological species for tissue engineering applications. Biocompatibility tests are in progress and will be discussed in a next paper.

Acknowledgments Wrigley Fibres (Somerset, United Kingdom) is kindly acknowledged for its supply of polyethylene particles. This work was funded by the National Research Project "PRIN 2003: The interface between silica-based materials and bio-molecules and/or molecular models."

References

1. P. SEPULVEDA, J. R. JONES and L. L. HENCH, *J. Biomed. Mater. Res.* **59** (2002) 340.
2. Y. LEE, Y. SEOL, Y. LIM, S. KIM, S. HAN, I. RHYU, S. BAEK, S. HEO, J. CHOI, P. KLOKKEVOLD and C. CHUNG, *J. Biomed. Mater. Res.* **54** (2001) 216–233.
3. P. SEPULVEDA, A. H. BRESSIANI, J. C. BRESSIANI, L. MESEGUER and B. KONIG, *J. Biomed. Mater. Res.* **62** (2002) 587–592.
4. E. A. B. KAUFMANN, P. DUCHEYNE and I. M. SHAPIRO, *J. Biomed. Mater. Res.* **52** (2000) 783–796.
5. J. C. BANWART, M. A. ASHER and R. S. HASSANEIN, *Spine* **20 (9)** (1995) 1055–1060.
6. J. A. GOULET, L. E. SENUNAS, G. L. DESILVA and M. L. GREENFIELD, *Clin. Orthop.* **39** (1997) 76–81.
7. J. PILITSIS, D. LUCAS and S. RENGACHARY, *Neurosurg. Focus* **13 (6)** Article 1 (2002).
8. G. A. HELM, H. DAYOUB and J. A. JANE, *Neurosurg. Focus* **10**(4, Article 4) (2001).
9. S. A. MASIELLO and J. A. EPSTEIN, Letter to regeneration Technologies, Inc. 6 Pooling of tissue from multiple donors during processing prohibited. Rockwille, MF: Food and Drug Administration (2001).
10. L. L. HENCH, *Curr. Opin. Sol. St. Mat.* **2** (1997) 604–610.
11. P. C. MCAFEE, B. W. CUNNINGHAM, D. O. ORBEGOSO, J. C. SEFTER, A. E. DMITREV and I. L. FEDDER, *Spine* **28 (4)** (2003) 332–340.
12. H. RAMAY and M. ZHANG, *Biomaterials* **24** (2003) 3293–3302.
13. P. SEPULVEDA, J. G. P. BINNER, S. O. ROGERO, O. Z. HIGA and J. C. BRESSIANI, *J. Biomed. Mater. Res.* **50** (2000) 27–34.
14. S. BOSE, J. DARSELL, M. KINTNER, H. HOSICK and A. BANDYOPADHYAY, *Mat. Sci. Eng. C* **23** (2003) 479–486.
15. O. GAUTHIER, J. M. BOULER, E. AGUADO, P. PILET and G. DACULSI, *Biomaterials* **19** (1998) 133–139.
16. Z. CONG, W. JIANXIN, F. HUAIZHI, L. BING and Z. XINGDONG, *J. Biomed. Mater. Res.* **55** (2001) 28–32.
17. M. VALLET-REGI, A. RAMILA, S. PADILLA and B. MUNOZ, *J. Biomed. Mater. Res.* **66** (2003) 580–585.
18. L. L. HENCH, *J. Biomed. Mater. Res.* **41** (1998) 511–518.
19. M. M. PEREIRA, A. E. CLARK and L. L. HENCH, *J. Biomed. Mater. Res.* **18** (1994) 693–698.
20. I. D. XYNOS, A. J. EDGAR, L. D. K. BUTTERY, L. L., HENCH and J. M. POLAK, *Biochem. Bioph. Res. Co.* **276** (2000) 461–465.
21. I. D. XYNOS, A. J. EDGAR, L. D. K. BUTTERY, L. L. HENCH and J. M. POLAK, *J. Biomed. Mater. Res.* **155 (2)** (2000) 151–157.

22. P. N. DE AZA, C. LUKLINSKA SANTOS, F. GUITINA and S. DE AZA, *Biomaterials* **24** (2003) 1437–1445.
23. E. CHARRIERE, J. LEMAITRE and P. H. ZYSSET, *Biomaterials* **24** (2003) 809–817.
24. J. JONES and L. L. LENCH, *Curr. Opin. Sol. St.* **7** (2003) 301–307.
25. O. LYCKFELDT and J. M. L. FERREIRA, *J. Eur. Cer. Soc.* **18** (1998) 131–140.
26. A. F. LEMOS and J. M. F. FERREIRA, *Mater. Sci. and Eng. C* **11** (2000) 35–40.
27. C. VITALE-BROVARONE, S. DI NUNZIO, O. BRETCANU and E. VERNÉ, *J. Mater. Sci. Mater. Med.* **15** (2004) 209–217.
28. C. VITALE-BROVARONE, E. VERNÉ, M. BOSETTI, P. APPENDINO and M. CANNAS, *J. Mater. Sci. Mater. Med.*, in press.
29. S. CALLCUT and J. C. KNOWLES, *J. Mater. Sci. Mate. Med.* **13** (2002) 485–489.
30. H. W. KIM, S. Y. LEE, C. J. BAE, Y. J. NOH, H. E. KIM and H. M. KIM, *et al.*, *Biomater.* **24** (2003) 3277–3284.
31. P. SEPULVEDA and J. G. P. BINNER, *J. Eur. Ceram. Soc.* **19** (1999) 2059–2066.
32. F. S. ORTEGA, P. SEPULVEDA, M. D. M. INNOCENTINI and V. C. PANDOLFELLI, *Am. Ceram. Soc. Bull.* **80 (4)** (2001) 37–42.
33. J. C. T. ANDRADE, J. A. CAMILLI, E. Y. KAWACHI and C. A. BERTAN, *J. Biomed. Mater. Res.* **62** (2002) 30–36.
34. V. S. KOMLEV and S. M. BARINOV, *J. Mater. Sci. Mater. Med.* **13** (2002) 295–299.
35. T. LIVINGSTON, P. DUCHEYNE and J. GARINO, *J. Biomed. Mater. Res.* **62** (2002) 1–13.
36. C. VITALE-BROVARONE and E. VERNÉ, *J. Mater. Sci. Mater. Med.*, in press.
37. T. KOKUBO, H. KUSHITANI and S. SAKKA, *J. Biomed. Mater. Res.* **24** (1990) 721–734.
38. O. PEITL, E. ZANOTTO and L. L. HENCH, *J. Non-Crys. Sol.* **292** (2001) 115–126.
39. S. FUJIABAYASHI, M. NEO, H. M. KIM, T. KOKUBO and T. NAKAMURA, *Biomaterials* **24** (2003) 1349–1356.
40. T. KOKUBO, H. M. KIM and M. KAWASHITA, *Biomaterials* **24** (2003) 2161–2175.
41. C. OHTSUKI, Y. AOKI, T. KOKUBO, Y. BANDO, M. NEO and T. NAKAMURA, *J. Ceram. Soc. Japan.* **103** (1995) 449–454.
42. C. KIM and S. JEE, *J. Eur. Cer. Soc.* **23** (2003) 1803–1811.
43. Z. SCHWARTS and B. D. BOYAN, *J. Cell. Biochem.* **56** (1994) 340–347.
44. H. YUAN, J. DE BRUIJN, X. ZHANG, C. VAN BLITTERSWIJK and K. DE GROOT, *J. Biomed. Mater. Res.* (*Appl. Biomater.*) **58** (2001) 270–276.
45. C. ZHANG, J. WANG, H. FENG, B. LU, Z. SONG and X. ZHANG, *J. Biomed. Mater. Res.* **54** (2001) 407–411.